

T. Kim

Department of Biomedical Engineering,
University of Michigan,
Ann Arbor, MI 48105

P. A. J. van Bakel

Department of Cardiac Surgery,
University of Michigan,
Ann Arbor, MI 48105

N. Nama

Department of Mechanical and
Materials Engineering,
University of Nebraska-Lincoln,
Lincoln, NE 68588

N. Burris

Department of Radiology,
University of Michigan,
Ann Arbor, MI 48105

H. J. Patel

Department of Cardiac Surgery,
University of Michigan,
Ann Arbor, MI 48105

D. M. Williams

Department of Radiology,
University of Michigan,
Ann Arbor, MI 48105

C. A. Figueroa

Department of Biomedical Engineering,
University of Michigan,
Ann Arbor, MI 48105;
Department of Surgery,
University of Michigan,
Ann Arbor, MI 48105

A Computational Study of Dynamic Obstruction in Type B Aortic Dissection

A serious complication in aortic dissection is dynamic obstruction of the true lumen (TL). Dynamic obstruction results in malperfusion, a blockage of blood flow to a vital organ. Clinical data reveal that increases in central blood pressure promote dynamic obstruction. However, the mechanisms by which high pressures result in TL collapse are underexplored and poorly understood. Here, we developed a computational model to investigate biomechanical and hemodynamical factors involved in Dynamic obstruction. We hypothesize that relatively small pressure gradient between TL and false lumen (FL) are sufficient to displace the flap and induce obstruction. An idealized fluid–structure interaction model of type B aortic dissection was created. Simulations were performed under mean cardiac output while inducing dynamic changes in blood pressure by altering FL outflow resistance. As FL resistance increased, central aortic pressure increased from 95.7 to 115.3 mmHg. Concurrent with blood pressure increase, flap motion was observed, resulting in TL collapse, consistent with clinical findings. The maximum pressure gradient between TL and FL over the course of the dynamic obstruction was 4.5 mmHg, consistent with our hypothesis. Furthermore, the final stage of dynamic obstruction was very sudden in nature, occurring over a short time (<1 s) in our simulation, consistent with the clinical understanding of this dramatic event. Simulations also revealed sudden drops in flow and pressure in the TL in response to the flap motion, consistent with first stages of malperfusion. To our knowledge, this study represents the first computational analysis of potential mechanisms driving dynamic obstruction in aortic dissection.

[DOI: 10.1115/1.4056355]

1 Introduction

1.1 Clinical Background. Thoracic aortic dissection (TAD) is characterized by a disruption of the intima, which leads to delamination of the aortic wall and creation of a true lumen (TL) and a false lumen (FL) [1]. Population-based studies have estimated that TAD occurs at a rate of 3–4 cases per 100,000 people per year [2,3]. TAD is commonly categorized using the Stanford classification, which distinguishes between type A aortic dissection, involving the ascending aorta, and type B aortic dissection (TBAD) which only involves the descending aorta [4]. One of the most dramatic complications of TAD is end-organ malperfusion, which is present in approximately 30% of type A aortic dissection and 20% of TBAD patients [5–7] and is associated with high morbidity and mortality [8,9]. Malperfusion is defined as inadequate flow to a vascular territory; if left untreated, it could result in malperfusion syndrome, which includes further complications such as tissue necrosis and end-organ dysfunction. Vessel malperfusion is caused by either dynamic obstruction, static obstruction, or a combination of both. Static obstruction occurs when the intimal flap extends into the branch vessel and causes fixed stenosis of the TL [10]. However, the pathophysiology of dynamic obstruction is

more complex. Clinically, we have observed two main drivers of dynamic obstruction. One is the high-pressure-related collapse described in this paper. The second is the abrupt relief of outflow obstruction and increase of TL outflow observed after restoration of flow by aortoiliac stenting can impose collapse of the infrarenal aorta TL. Stenting that segment can in turn cause collapse of the TL supplying the celiac and superior mesenteric artery (SMA). Focused on the first case, we hypothesized that dynamic obstruction is driven by FL pressure exceeding TL pressure, causing the flap to drape over the ostium of a branch vessel supplied by the TL and thus obstruct blood flow.

While dynamic obstruction has been reported in prior clinical studies, the factors driving this phenomenon remain unknown, largely due to the challenges of assessing pressure in TL and FL during dynamic obstruction, at a time when restoration of normal branch-artery perfusion pressures is the highest clinical priority. Computational simulations can be used to shed light on this phenomenon via in-silico investigations of the intimal flap motion and its relation to the pressure gradient across TL and FL.

1.2 Clinical Example of Dynamic Obstruction. A 36-year-old hypertensive female with renal failure (blood pressure 170/80, creatinine 4.2 mg/dL) presented with TBAD. To correct hypertension, intravenous hydralazine, and esmolol were administered. To determine whether there was a treatable anatomical cause of the

Manuscript received June 6, 2022; final manuscript received November 18, 2022; published online December 21, 2022. Assoc. Editor: Kyle Quinn.

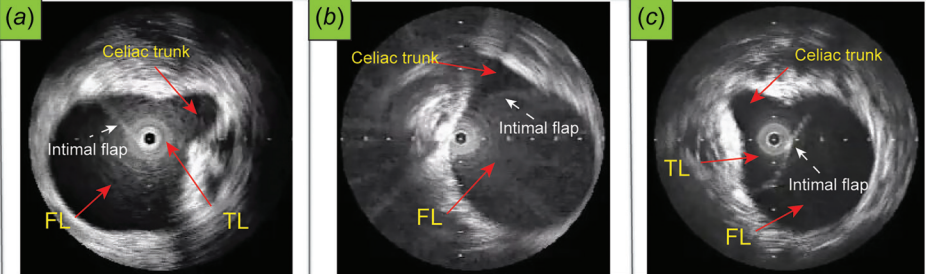
IVUS			
	Patent TL		TL obstructed (Dynamic obstruction)
	Esmolol infusion	Esmolol discontinued. Hypotension treated medically and patient intubated	Esmolol infusion resumed
	Time [h:min]		20:53
	P [mmHg]		93/53

Fig. 1 Timeline of dynamic obstruction and blood pressure during baseline infusion of esmolol: (a) following discontinuation of esmolol and after intubation, (b) and after vasodilator infusion and esmolol resumption, (c) TL = true lumen, FL = false lumen, and P = abdominal aorta TL blood pressure

hypertension, angiograph, and intravascular ultrasound examinations were performed. Intraluminal blood pressure was assessed in the FL using an arterial catheter. Aortic root pressure was compared with abdominal aorta TL, visceral, and iliac artery pressures. Aortic root and abdominal TL pressures were both 90/50 and the TL was approximately $\frac{1}{4}$ of the total aortic cross section (Fig. 1(a)). No pressure deficits were present in the celiac trunk or SMA, Renal artery systolic pressure deficits (compared to the aortic root and measured distal to dissection reentry tears) were 70 mm Hg on the right and 15 on the left. While the operators were preparing to stent the right renal artery, the patient became hypoxic and developed sinus bradycardia with oxygen saturation in the low 80s and a heart rate of 46 bpm. In view of impending respiratory arrest, esmolol was stopped, fluids were administered, and a medical code was called. The code team administered Romazicon (a sedative reversal agent) and atropine (to increase heart rate), and intubated the patient. After fluids and discontinuation of esmolol, cuff blood pressure rose to 110/50, further increasing to 200/102 after intubation. Intravascular ultrasound examination, while abdominal aorta TL blood pressure was 159/83, demonstrated TL collapse with the intimal flap draped over and prolapsing into the ostia of the celiac trunk and SMA (Fig. 1(b)). Esmolol was subsequently restarted resulting in normalization of blood pressure (93/53 mmHg) and displacement of the flap away from the branch vessel ostia, reestablishing flow to the abdominal aorta TL, celiac trunk, and SMA (Fig. 1(c)).

1.3 Previous Computational Studies on the Aortic Dissection. No computational study has thus far investigated aortic dynamic obstruction and malperfusion. Previous contributions have been focused on characterizing complex hemodynamics in aortic dissection, often using patient-specific models with rigid wall assumptions. Some studies have investigated the effects of antihypertension medication on hemodynamic parameters [11,12]. Other studies have explored the factors determining FL thrombosis and retrograde aortic dissection [13,14]. Healthy and acutely dissected aortas were compared to understand the effects of dissection geometry on aortic hemodynamics [15]. Other studies have focused on the effect of connecting tears, including tear size and location [16]. Reentry tears were also found to have a large effect on pressure and flow distributions between the TL and FL [15]. Other anatomical risk factors such as curvature were also

investigated for type B aortic dissection using idealized models [17]. Rigid wall models were also used to quantify the pressure difference between the TL and FL. This difference was found to be smaller than 20 mmHg in a patient-specific analysis [18].

A rigid wall representation of the intimal flap assumes fixed flap position, and, therefore, is unsuitable to relate flap motion with pressure gradient between TL and FL. Noting this, fluid–structure–interaction (FSI) models have been used in aortic dissection simulations to investigate the effect of the intimal flap motion on hemodynamic parameters. Compared to analyses under rigid wall assumptions, FSI simulations are challenging because of the high complexity and computational cost of the problem, which deals with the coupled motion of the fluid and solid [19,20]. An FSI model with rigid intimal flap calculated a peak systolic 30 mmHg pressure difference between TL and FL [20]. Several studies focused on studying the differences in wall shear stress between rigid wall and FSI simulations [19,21].

Finally, intimal flap motion was investigated in several studies. Several studies reported small flap displacements (0.15–1 mm) after imposing different levels of pressure difference between TL and FL [19,22,23]. More recently, another study investigated the impact of intimal flap material stiffness on flap displacement. Imposing a 5 mmHg pressure difference between TL and FL, flap displacement varied from 1.4 mm to 13.4 mm as the flap material stiffness varied from 20 kPa to 800 kPa, respectively [24].

However, to the best of our knowledge, no studies so far have investigated dynamic obstruction and malperfusion caused by flap motion.

1.4 Hypothesis and Purpose. In this work, we aimed to investigate the biomechanical and hemodynamic factors driving dynamic obstruction in aortic dissection. The above clinical example showed that an increase in systemic blood pressure was associated with dynamic obstruction. Furthermore, pharmacologic management of systemic blood pressure resulted in restoration of TL patency. From a clinical perspective, it is not feasible to assess TL and FL pressure during dynamic obstruction. In this study, we hypothesized that relatively small pressure differentials between the TL and FL are sufficient to displace the flap and induce obstruction because of the highly compliant nature of the intimal flap, concurrent with a global increase in systemic blood pressure. To test this hypothesis, we developed an FSI model of dynamic obstruction in TBAD, whereby inducing dynamic changes in systemic blood pressure were triggered by altering FL outflow resistance.

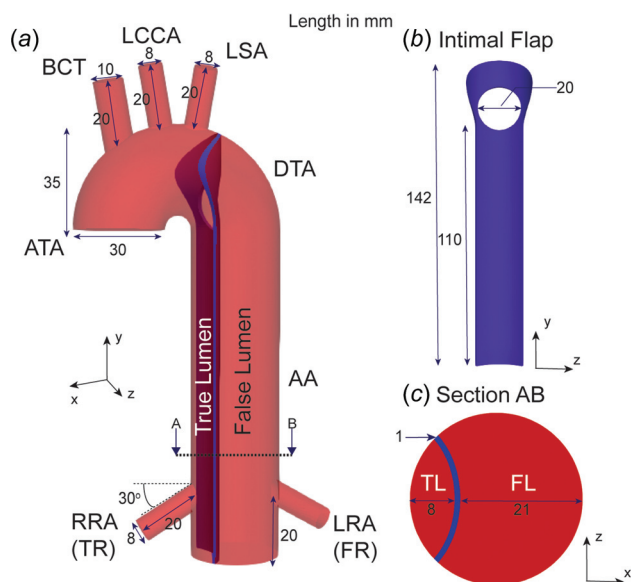


Fig. 2 Idealized 3D geometrical model of a TBAD. Fluid and solid domains are depicted in red and blue, respectively. Dimensions in mm. ATA: ascending thoracic aorta, DTA: descending thoracic aorta, AA: abdominal aorta.

2 Methods

2.1 Geometrical Model. An idealized three-dimensional (3D) geometrical model of a TBAD was constructed (Fig. 2). The model consists of fluid and solid domains (noted in red and blue, respectively). The fluid domain consists of the aorta and main branch vessels. The uniform aortic diameter and length are 30 and 173 mm, respectively. The model includes the ascending thoracic aorta, descending thoracic aorta, and abdominal aorta. The branch vessels include the brachiocephalic trunk (BCT), left common carotid artery (LCCA), left subclavian artery (LSA), and right and left renal arteries (RRA and LRA). BCT diameter is 10 mm. All other branch vessels have an 8 mm diameter. All branch lengths are 20 mm. The RRA is perfused by the TL and the LRA is perfused by the FL. Thus, from now on, we refer to the RRA and LRA branches as true lumen renal artery (TR) and false lumen renal artery (FR) branches, respectively.

The solid domain represents the intimal flap (Fig. 2(b)). A single 20 mm diameter circular entry tear and no reentry tears were assumed. The aortic walls were assumed to be rigid. The intimal flap has a 1 mm uniform thickness and a total length of 142 mm. The flap has a constant curvature along the axial direction and divides the descending thoracic aorta and abdominal aorta into a TL and a FL with areas of 113 mm² and 570 mm², respectively. The distance between the intimal flap and aortic wall of TL and FL are 8 mm and 21 mm, respectively (Fig. 2(c)).

2.2 Governing Equations and Assumptions. Arbitrary Lagrangian–Eulerian formulation was used for the FSI simulation. Blood was modeled as an incompressible Newtonian fluid, and the intimal flap as a homogenous, isotropic, nearly incompressible Neo-Hookean material. Simple linear elasticity model does not make a good description of deformation with large strain. In order to analyze the large motion of the intimal flap during dynamic obstruction and decrease the computational cost, we used a Neo-Hookean model, which is a simple nonlinear elasticity model. The incompressible Navier–Stokes equations in a moving domain and the elasto-dynamics equations were simultaneously solved in COMSOL MULTIPHYSICS 5.6.1, rendering solutions for blood velocity v_{fluid} and pressure p , and intimal flap displacement u_{solid} . Using an Arbitrary Lagrangian–Eulerian formulation, the Navier–Stokes equations are written in a moving mesh that follows the motion of

the intimal flap interface (body-fitted mesh). Mesh motion was solved in every time-step assuming a Yeoh hyper-elastic constitutive model with boundary conditions that matched the motion intimal flap interface. Blood density ρ and dynamic viscosity μ were set to 1060 kg/m³ and 0.004 Pa·s, respectively. The strain energy density W_s for the intimal flap is

$$W_s = \frac{1}{2} \mu (I_1 - 3) - \mu \ln(J) + \frac{1}{2} \lambda \ln(J)^2 \quad (1)$$

where I_1 is the first invariant of the right Cauchy–Green deformation tensor $\mathbf{C} = \mathbf{F}^T \mathbf{F}$, $J = \det(\mathbf{F})$ is the third invariant of the deformation gradient tensor \mathbf{F} , and μ and λ are Lamé parameters

$$\mu = \frac{E}{2(1+\nu)}, \quad \lambda = \frac{E}{3(1-2\nu)} \quad (2)$$

where E is the Young's modulus, and ν is the Poisson's ratio. Due to the lack of experimental data, in this study, we assumed that the flap is less stiff than the thoracic aorta [25]. The rationale for this assumption is that the inner layer of the aortic wall from where the flap originates consists primarily of elastin fibers, which are more compliant than the collagen fibers more prevalent in outer layers of the aortic wall [26]. Therefore, given that the material stiffness of the descending thoracic aorta and abdominal aorta has been reported as 0.5–1 MPa and 1.5–2 MPa, respectively [25], we assumed Young's modulus for the intimal flap of 0.1 MPa. The flap density was set to 1080 kg/m³ and its Poisson's ratio ν to 0.49.

2.3 Boundary Conditions. A steady-state flowrate ($Q_{\text{in}} = 6 \text{ L/min}$) boundary condition, mapped to a parabolic profile, was set at the inlet face of the aortic model. Pulsatility was neglected because the time scale of dynamic obstruction is several minutes (Fig. 1), much longer than the time scale of a single cardiac cycle ($\sim 1 \text{ s}$). Flowrate conditions were prescribed at BCT, LCCA, and LSA vessel branches (outlets 1–3 in Fig. 3) as a fixed % of the cardiac output: 16.6%, 8.5%, and 8.1%, respectively [27].

Resistance outlet boundary conditions were set for TR branch, FR branch, TL, and FL (outlets 4–7), (Fig. 3(b)). Initial resistance values for each branch were set as $R = \Delta P / Q$, based on $\Delta P = 94 \text{ mmHg}$ for outlets 4–7, and flowrates (Q) of 0.1 Q_{in} for TR and FR branches [27], 0.14 Q_{in} for TL, and 0.328 Q_{in} for FL. This ratio of flows in TL:FL assumes that, initially, 30% of the flow goes through the TL and 70% through the FL. While TR branch, FR branch, and TL resistances were kept constant over time, the FL resistance was dynamically controlled. After 10 s, a linear increase of FL resistance was imposed. The increase in FL resistance triggered both a systemic increase in blood pressure and also the intimal flap motion. Table 1 summarizes the resistance values used in the simulation. The outer aortic walls were assuming to be rigid.

Finally, all edges of the solid domain were kept fixed, including the edge at the distal end of the flap, on the outflow face of the computational domain.

2.4 Discretization and Simulation. The fluid and solid domains were discretized using tetrahedral elements. A second-order backward differentiation formula time integration method was used. Mesh independence studies were conducted using three different computational grids containing 0.34 M, 0.67 M, and 1.4 M elements. Convergence was achieved for the quantities of interest (for instance, maximum intimal flap displacement changed by only 4% between the 0.67 M and 1.4 M element meshes) for the 1.4 M element mesh, which consists of 1,363,198 fluid and 38,323 solid elements and 243,028 fluid and 11,217 solid nodes. FSI simulations were run using COMSOL MULTIPHYSICS 5.6.1.

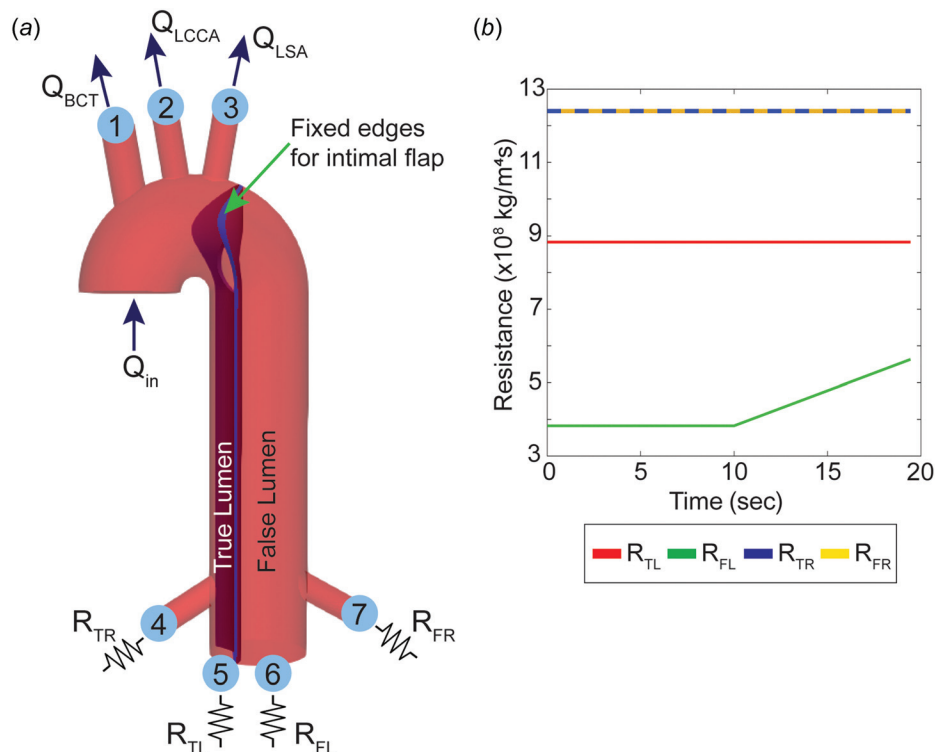


Fig. 3 (a) Schematic of boundary conditions for the fluid and solid domains and (b) imposed histories of outlet resistances

Table 1 Resistance values used in TR, FR, TL, and FL

Outlet face	Outlet number	Resistance ($\times 10^8 \text{ kg/m}^4\text{s}$)
TR branch	4	12.40
FR branch	7	12.40
TL	5	8.83
FL	6	$\begin{cases} 3.82, 0 < t < 10 \text{ s} \\ 0.192t + 1.9, t > 10 \text{ s} \end{cases}$

The simulation ran for 35 h on 36 cores of Intel® Xeon® CPU E5-2699, 124 GB RAM, running UBUNTU 20.04.

3 Results

3.1 Intimal Flap Displacement. Figure 4 shows plots of intimal flap displacement at the Π plane ($y = 18 \text{ mm}$, panel a) and Ω plane ($z = 0 \text{ mm}$, panel b) at $t = 0 \text{ s}$ and at time $t = 19.44 \text{ s}$ (final time, corresponding to the start of dynamic obstruction of the TR branch). The Π plane corresponds to the position of maximum flap displacement for all time points of the simulation. At $t = 0 \text{ s}$, the maximum flap displacement is 0.4 mm , TL and TR branch are fully patent, and the areas of TL and FL are 109 mm^2 and 574 mm^2 , respectively.

The prescribed dynamic increase in FL resistance increases FL pressure and thus induces a motion of the intimal flap toward the TL wall, ultimately resulting in dynamic obstruction of the TR branch. At the last time-step of the analysis ($t = 19.44 \text{ s}$), the maximum intimal flap displacement is 7.8 mm , nearly identical to the initial distance between TL wall and intimal flap of 8 mm (see Fig. 2(c)). The TL and FL area at the final time-step are 17.3 mm^2 and 665.3 mm^2 , respectively. The TL area reduction is 84% . Simulations of the intimal flap motion beyond the final time-step ($t = 19.44 \text{ s}$) require incorporation of a contact model

within our computational framework and were not considered in this study.

3.2 Pressure and Velocity Contours. Figure 5 shows contours of pressure (panel a) and velocity (panel b) at $t = 0 \text{ s}$ and $t = 19.44 \text{ s}$. At $t = 0 \text{ s}$, mean inflow aortic pressure is 95.7 mmHg , and the pressure difference between FL and TL is smaller than 0.5 mmHg . A region of high pressure is apparent in the FL of the proximal descending aorta, where the high-velocity flow through the tear impinges against the FL wall.

The prescribed increase in FL resistance results in an increase in total systemic resistance and a corresponding increase in systemic blood pressure (since the cardiac output remains constant). The mean inflow aortic pressure at $t = 19.44 \text{ s}$ is 115.3 mmHg . Simulation results, therefore, reproduce a global increase in pressure (from 95.7 mmHg to 115.3 mmHg) as the intimal flap collapsed onto the TL and occluded the TR branch. This behavior is consistent with the clinical example reported in Fig. 1.

Furthermore, as the FL resistance and global pressure increased, so did the pressure difference between FL and TL, from 0.5 mmHg at $t = 0 \text{ s}$, to 4.5 mmHg at $t = 19.44 \text{ s}$. This 4.5 mmHg pressure difference is only 3.9% of the central aortic pressure (115.3 mmHg) and thus is challenging to assess in vivo as dynamic obstruction unfolds.

At $t = 0 \text{ s}$, the maximum TL velocity is 42 cm/s . As the intimal flap moves toward the TL wall, the TL area decreases, and its velocity increases. A maximum TL velocity of 118.5 cm/s occurs at the gap between the intimal flap and the TL aortic wall at time $t = 19.44 \text{ s}$. The velocity at the ascending thoracic aorta and upper branches remain relatively constant due to the fixed flowrate boundary conditions at BCT, LCCA, and LSA.

3.3 History of Hemodynamic Indices. Figure 6 shows temporal plots for resistance, blood pressure, and flowrate at TL, FL, and TR and FR branches, in addition to pressure difference

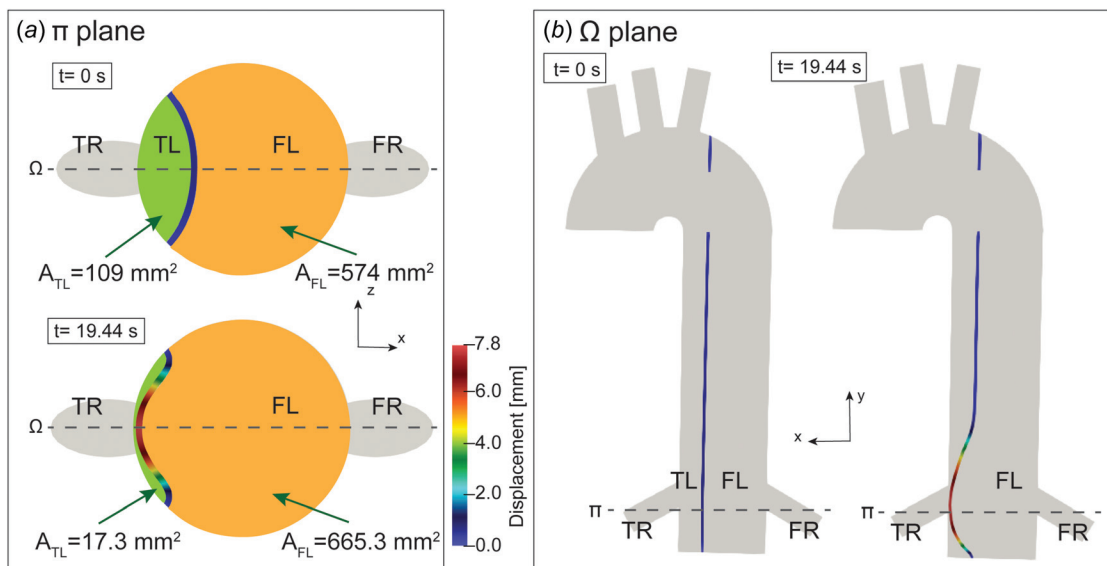


Fig. 4 Intimal flap displacement at times $t = 0$ and $t = 19.44$ s at (a) Π plane ($y = 18$ mm) and (b) Ω plane ($z = 0$ mm)

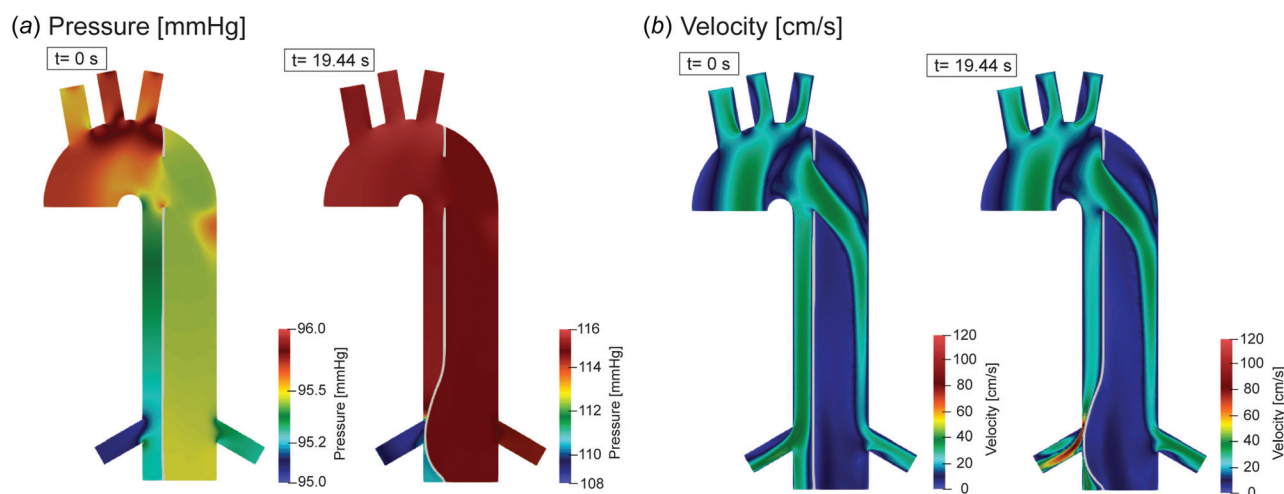


Fig. 5 (a) Pressure and (b) velocity contour at $t = 0$ and $t = 19.44$ s

between FL and TL and maximum intimal flap displacement at the plane Π . Temporal plots show three distinct stages: steady-state (0–10 s), development (10–19 s), and obstruction (19–19.44 s). These stages are clearly appreciated in the FL-TL pressure difference (panel c).

During the steady-state stage, resistances at TL, FL, TR, and FL are constant and therefore no dynamic changes are observed in the hemodynamics. During the development stage, FL resistance is increased linearly while keeping the other resistances fixed. The displacement of the intimal flap is limited during this stage (see panel e), from 0.4 mm at $t = 10$ s to 2.1 mm at $t = 19$ s. The pressure gradient between FL and TL also mildly increases during this stage, from 0.42 mmHg at $t = 10$ s, to 0.58 mmHg at $t = 19$ s (panel c). Due to the prescribed increased in FL resistance, FL flowrate decreases from 1.99 to 1.62 L/min and flow rates through TL, and TR and FR branches increase (panel d).

During the obstruction stage, the intimal flap gets dramatically closer to the TL aortic wall: its displacement increases from 2.1 mm to 7.8 mm in just 0.44 s. At this point, the flap movement causes obstruction of the TL and the TR branch (see Fig. 4). As a result of the obstruction, there is a sudden drop of pressure and

flowrate in the TL and TR branch (Fig. 6 panel b and d, respectively). Conversely, FL and FR branch flows increase. The increase in FL flow happens despite the continuous (imposed) increase in FL resistance. Pressure difference between FL and TL rapidly increases in the obstruction stage, from 0.58 mmHg at $t = 19$ s, to 4.5 mmHg at $t = 19.44$ s (panel c).

4 Discussion

In this study, we have demonstrated that computational simulations can be used to understand the complex hemodynamics associated with dynamic obstruction in type B aortic dissection. Specifically, we performed a detailed characterization of both TL and FL hemodynamics which cannot be easily assessed in vivo. Our results have revealed that in our model dynamic obstruction occurred as mean systemic blood pressure increased from 95.7 mmHg to 115.3 mmHg (Fig. 5 panel a). This behavior is consistent with the clinical example reported in Fig. 1, where dynamic obstruction occurred as mean systemic blood pressure increased from 63.3 mmHg to 108.3 mmHg, although the exact transition pressure was not documented. Our clinical experience

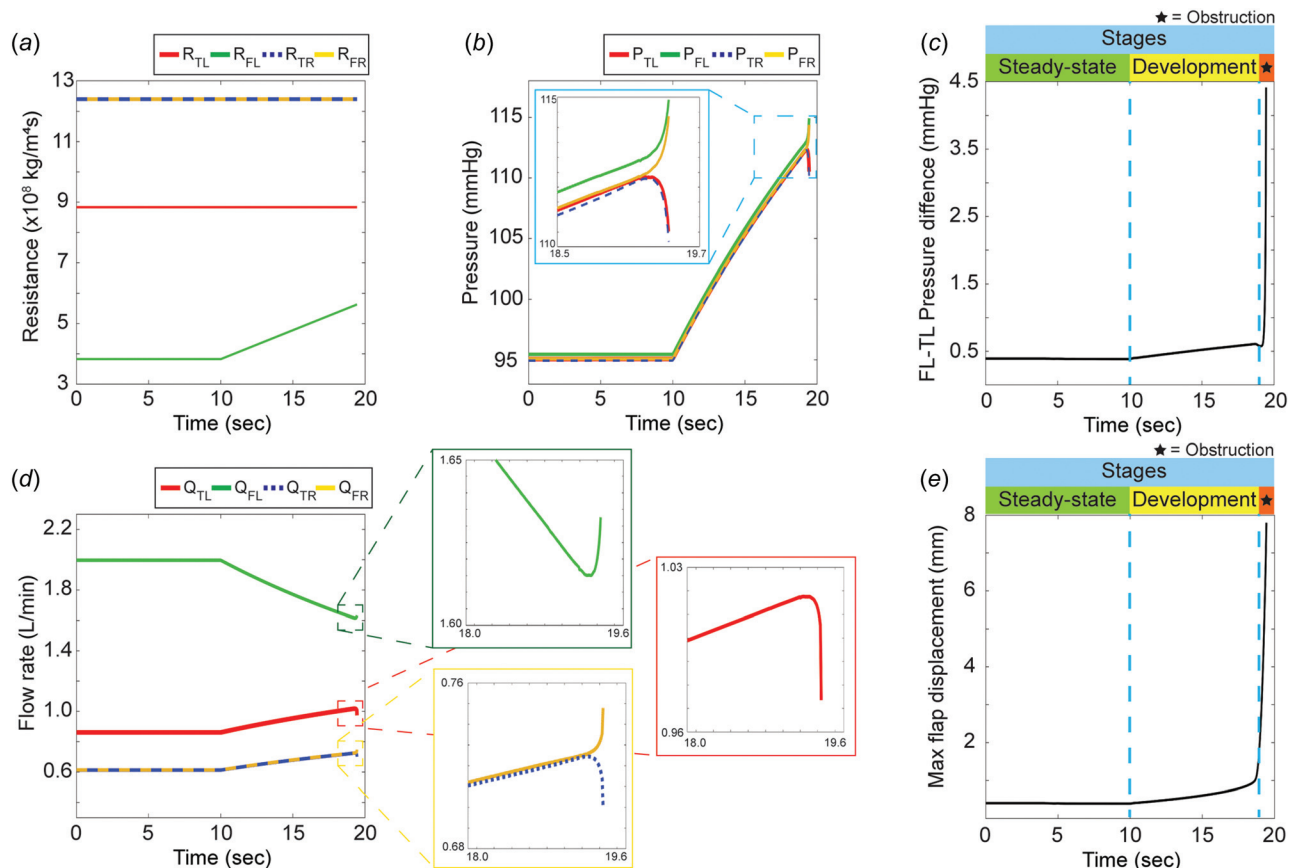


Fig. 6 Time history of (a) resistance, (b) pressure, (c) pressure difference between TL and FL, (d) flow, and (e) maximum flap displacement. Resistance, pressure, and flow are given for TL, FL, TR, and FR branches. Pressure difference between FL and TL is given at the aortic outlet, and maximum flap displacement is given at plane II.

has shown that the transition-pressure window in patients has been as low as 75 mm Hg and as narrow as 10–15 mm Hg.

Our results have supported the hypothesis that relatively small pressure differences between FL and TL are sufficient to displace the flap to induce dynamic obstruction. Here, a maximum FL–TL pressure difference of 4.5 mmHg was obtained just before the complete TL obstruction. During most of the dynamic obstruction, the FL–TL pressure differences remained under 1 mmHg, and only in the instances just before obstruction did the pressure differences increase substantially.

Clinically, increases in central blood pressure may be triggered by a variety of mechanisms, including hypertension, partial thrombosis in the FL, hypoxia, changes in vasoactive medication administration, etc. [28–30]. In this simulation, these changes were reproduced by imposing an increase in FL resistance while keeping the cardiac output and other outflow boundary conditions (prescribed flows and resistances) constant.

Our results have shown that the final stage of dynamic obstruction was very sudden in nature, occurring over a short time (<1 s, see Fig. 6), consistent with the clinical understanding of this dramatic event. The TL remained patent as pressure differentials between FL and TL slowly changed until a threshold was reached and sudden obstruction occurred. This threshold for sudden obstruction may vary with the patients' age, vascular anatomy, and chronicity of the intimal flap.

We have often observed onset of dynamic obstruction in the abdominal aorta accompanied by TL collapse following correction of static obstruction of the aortoiliac segment. However, we submit that whatever the trigger for transient changes in hemodynamic conditions might be, such as alterations in cardiac output, differential resistances in TL- and FL-supplied branch arteries or different numbers and sizes of connecting tears, etc.,

it only takes a relatively small pressure difference between FL and TL to induce intimal flap motion and ultimately TL obstruction. In this study, we have demonstrated the clear association between systemic changes in blood pressure and dynamic obstruction.

4.1 Material Stiffness of the Intimal Flap. To date, no human or animal experimental studies have reported the material stiffness of the intimal flap. Previous computational studies used different assumptions: Alimohammadi [19], and Qiao [23] assumed the same material stiffness for intimal flap and aortic wall. Another study considered a wide range of material stiffness (0.02–0.80 MPa) and tried to match the flap displacement observed in the clinical images [24].

In this study, we assumed that the flap is less stiff than the thoracic aorta [25]. This assumption is justified because the flap consists primarily of elastin fibers, which are more compliant than the collagen fibers more prevalent in outer layers of the aortic wall [26]. Also, the phenomenon of pressure-related TL collapse has only been observed clinically in days-old aortic dissections, in which the acute dissection flap is thin and flimsy. Dissection flaps in dissections weeks to months old are in various states of thickening due to fibrosis and have not been observed to behave in this same way. We have not observed dynamic obstruction in a single instance of chronic dissection.

Considering this, several simplifying assumptions were made to set the mechanical properties of the intimal flap. Material stiffness and thickness were assumed to be uniform along its length. The flap thickness was set to 1 mm. As for the material stiffness, we considered values in the 0.07–0.50 MPa range. Ultimately, a 0.10 MPa value was used. This value enabled us to reproduce

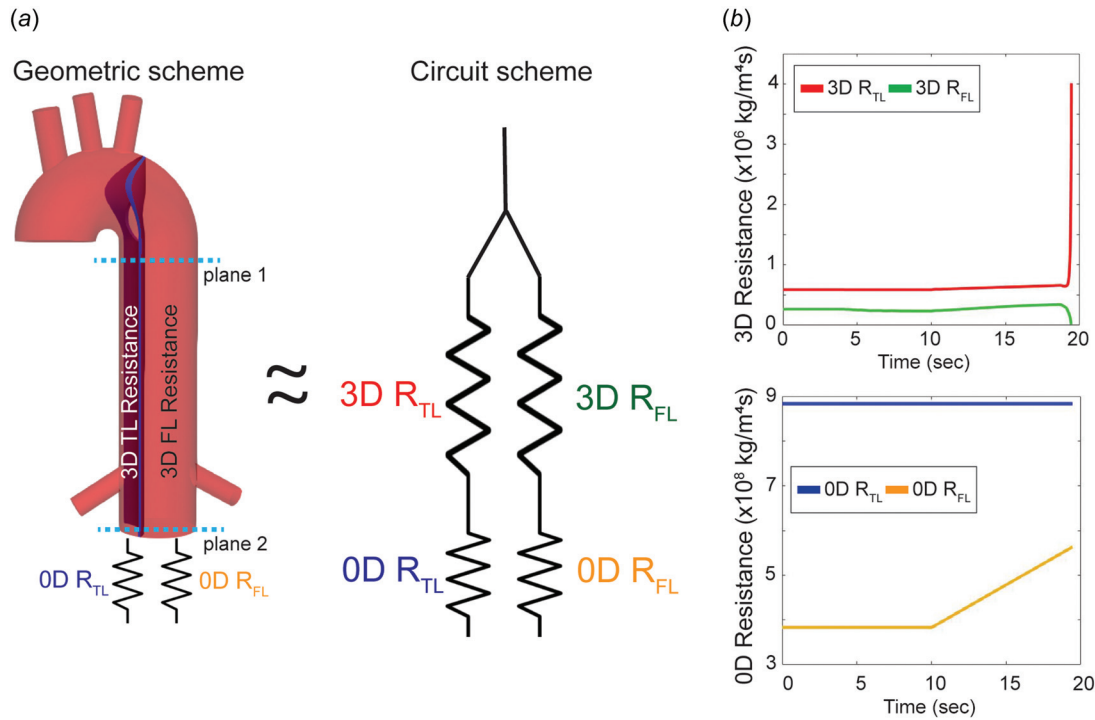


Fig. 7 (a) Schematic decomposition of TL and FL resistance into a 3D geometric and a 0D distal components acting in series for each lumen and (b) Time history of 0D and 3D geometric TL and FL resistances

physiologic changes in mean pressure over the course of the dynamic obstruction. When the flap stiffness was too low (~ 0.07 MPa), the dynamic obstruction was triggered at lower levels of pressure. Conversely, dynamic obstruction occurred at elevated levels of systemic blood pressure when the intimal flap material stiffness was large (~ 0.50 MPa). In reality, one would expect changes in material stiffness and thickness (and therefore in structural stiffness [31]) along the length of the flap.

4.2 Distal (Zero-Dimensional) and Geometric (Three-Dimensional) Changes in Vessel Resistance. To understand the hemodynamic changes during dynamic obstruction, it is helpful to consider two types of resistances for each lumen: (1) the zero-dimensional (0D) distal resistance imposed via boundary conditions, and (2) the 3D geometrical resistance, which varies over time due to changes in cross-sectional area (see schematic in Fig. 7). The 3D geometrical resistance can be evaluated as $R = \Delta P/Q$ for both TL and FL, where ΔP is the pressure differential between planes 1 and 2, and Q is the flow in each lumen. For each lumen, the total resistance is thus the sum of the 3D geometrical and the 0D distal components (see panel a of Fig. 7).

During the steady-state (0–10 s) and development (10–19 s) stages, there are no significant changes in TL and FL 3D resistances (Fig. 7 panel b). Therefore, the prescribed increase in FL 0D resistance causes a decrease in FL flow (Fig. 6 panel d). In the obstruction stage (19–19.44 s), as the intimal flap moves toward the TL wall, significantly reducing the TL area, the 3D geometrical resistances change substantially: the 3D TL resistance increases six-fold, from 0.65×10^6 at $t = 19$ s, to 4.00×10^6 kg/m⁴s at $t = 19.44$ s (Fig. 7 panel b). This increased 3D TL resistance is associated with a reduction in TL flow and an increased FL flow (Fig. 6 panel d) despite the prescribed increased in FL 0D resistance.

This study underlines the relationship between alterations in peripheral vascular resistance (represented here by 0D circuits) and dynamic TL collapse. Optimal pharmacological management of these patients induces changes in peripheral vascular resistance that may impact the overall pressure levels in TL and FL and thus potentially trigger dynamic obstruction.

4.3 Auto-Regulation of the Branch Vessels. In this study, flow to the upper branch vessels was assumed constant over time, and renal artery outflows were determined via fixed resistance boundary conditions. Both the cerebral and the renal circulations are heavily autoregulated and thus have the capacity of maintaining flow over a wide range of systemic pressures [32–35]. Setting a fixed flow boundary conditions effectively achieved this behavior for the upper branch vessels. However, for the renal arteries, setting a fix flow condition was not a reasonable modeling choice as we wanted to study malperfusion during dynamic obstruction. As a result, both renal flows varied over time corresponding to the systemic blood pressure change (Fig. 6). Future studies will expand on the work presented here by accounting for renal flow autoregulation models, which attempt to maintain constant flow over a 90–170 mmHg range of systemic blood pressures [36].

4.4 Flow Distribution Between True Lumen and False Lumen. In this study, a 30:70 TL:FL flow ratio was assumed. Different flow ratios would impact the simulation results. With a 30:70 TL:FL flow ratio, dynamic obstruction occurred at systemic blood pressure of 115.3 mmHg. As more flow goes through the TL for a given TL:FL area ratio, the pressure drop between aortic root and distal TL increases, resulting in larger pressure differentials between FL and TL. We tested a 50:50 TL:FL flow ratio with the same geometry. Here, dynamic obstruction occurred at lower levels of systemic pressure (101.5 mmHg). Furthermore, the TL:FL ratio of flows and areas may vary considerably across patients. The ratios of TL:FL peak flows ranged from 0.5 to 2 in Dillon-Murphy [15] and Baumlér [24], respectively. Both patients had larger FL than TL. Anatomical variation, such as different TL:FL area ratios, the size and number of initial and reentry tears, and the patency of the FL can alter the TL:FL flow distributions across patients.

4.5 Limitations. Lack of a contact model: Due to a lack of contact model, simulations stopped at the time-step ($t = 19.44$ s) when the intimal flap nearly touched the TL wall. When contact occurs, the topology of the fluid domain changes: the TL is no

longer a continuous conduit, and contact forces between intimal flap and TL wall must be defined. These additional complexities were outside the scope of this work, which was focused on describing the temporal response of dynamic obstruction in aortic dissection. In the future, will tackle this TL collapse using other FSI strategies relying on immerse-boundary formulations [37].

Lack of reentry tears: In this study, we assumed no reentry tears in the model. However, studies have shown that patients with aortic dissection have an average of 2–3 reentry tears. The most common locations for reentry tears are the descending aorta and the juxta-renal region [38,39]. Previous research showed the significant effects of reentry tears on aortic dissection hemodynamics. A larger number of reentry tears tends to equilibrate the pressure between TL and FL [15]. Based on this principle, dynamic obstruction can be treated by fenestration. Size and location of reentry tears, such as near side branches, are also likely to impact dynamic obstruction.

Rigid aortic wall assumption: To reduce complexity and computational cost, we modeled the behavior of the aortic wall as rigid and only studied the FSI problem given by the interactions between flow in TL and FL and a deformable intimal flap. However, the aorta experiences relatively large deformation, even in patients with relatively stiffer vessels [35,40,41]. This deformability affects flow through TL and FL, which in turn will affect intimal flap motion. Compliant outer walls may impact the dynamics of flap motion due to the differential ability that TL and FL have to accommodate changes in blood volume as blood pressure changes. These changes may be important if pulsatility is considered in the FSI simulation. Here, the assumed steady-state flow conditions reduce the impact of this simplifying assumption. Future expansions on this work will account for aortic wall deformation.

Lack of pulsative flow: Nonpulsatile flow was used for this study because the time scale of dynamic obstruction is several minutes (Fig. 1), much longer than the time scale of a single cardiac cycle (~ 1 s). However, under pulsatile conditions, the pressure difference between FL and TL will also be pulsatile and therefore the flap displacement may also exhibit a pulsatile component superimposed with the steady-state trend described in this work. Additionally, it is possible for a transitional stage to occur whereby TL collapse happens only during systole, but not in diastole. This situation could only be studied by simulating dynamic obstruction under full pulsatile conditions.

Idealized anatomy: a highly simplified type B aortic dissection model was used for this study. More complex anatomical features such as vessel tortuosity and curvature, in addition to the number of reentry tears, may affect dynamic obstruction. From a clinical perspective, it would be interesting to investigate whether there is a particular dissection anatomy prone to dynamic obstruction. Further work will involve correlating anatomical features such as entry tear size, tear location, aortic curvature, constellation of branch arteries compromised by static obstruction, etc.

5 Conclusion

An idealized FSI type B aortic dissection model was created to study dynamic obstruction. Our model succeeded in reproducing the clinical evidence supporting that dynamic obstruction occurs as mean systemic blood pressure increases. Our results showed that relatively small pressure differences between FL and TL are sufficient to displace the intimal flap to induce dynamic obstruction. Finally, the final stage of dynamic obstruction occurred over a very short time (< 1 s), consistent with the clinical understanding of this dramatic event. To our knowledge, this study shows the first computational analysis of potential mechanisms driving dynamic obstruction in aortic dissection.

Acknowledgment

This work was supported by the Edward B. Diethrich Professorship; the Joe D. Morris Collegiate Professorship; the Family of

Harpreet and Sangeeta Ahluwalia Fund; the David Hamilton Fund; the Aikens Aortic Grants Program and the University of Michigan Frankel Cardiovascular Center.

Data Availability Statement

The datasets generated and supporting the findings of this article are obtainable from the corresponding author upon reasonable request.

References

- [1] Goldfinger, J. Z., Halperin, J. L., Marin, M. L., Stewart, A. S., Eagle, K. A., and Fuster, V., 2014, "Thoracic Aortic Aneurysm and Dissection," *J. Am. Coll. Cardiol.*, **64**(16), pp. 1725–1739.
- [2] Meszaros, I., Morocz, J., Szilavi, J., Schmidt, J., Tornoci, L., Nagy, L., and Szép, L., 2000, "Epidemiology and Clinicopathology of Aortic Dissection," *Chest*, **117**(5), pp. 1271–1278.
- [3] Peterss, S., Mansour, A. M., Ross, J. A., Vaitkeviciute, I., Charilaou, P., Dumfarth, J., Fang, H., Ziganshin, B. A., Rizzo, J. A., Adeniran, A. J., and Elefteriades, J. A., 2016, "Changing Pathology of the Thoracic Aorta From Acute to Chronic Dissection: Literature Review and Insights," *J. Am. Coll. Cardiol.*, **68**(10), pp. 1054–1065.
- [4] Daily, P. O., Trueblood, H. W., Stinson, E. B., Wuerflein, R. D., and Shumway, N. E., 1970, "Management of Acute Aortic Dissections," *Ann. Thorac. Surg.*, **10**(3), pp. 237–247.
- [5] Geirsson, A., Szeto, W. Y., Pochettino, A., McGarvey, M. L., Keane, M. G., Woo, Y. J., Augoustides, J. G., and Bavaria, J. E., 2007, "Significance of Malperfusion Syndromes Prior to Contemporary Surgical Repair for Acute Type A Dissection: Outcomes and Need for Additional Revascularizations," *Eur. J. Cardio-Thorac. Surg.*, **32**(2), pp. 255–262.
- [6] Fattori, R., Tsai, T. T., Myrmel, T., Evangelista, A., Cooper, J. V., Trimarchi, S., Li, J., Lovato, L., Kische, S., Eagle, K. A., Isselbacher, E. M., and Nienaber, C. A., 2008, "Complicated Acute Type B Dissection: Is Surgery Still the Best Option? A Report From the International Registry of Acute Aortic Dissection," *JACC Cardiovasc. Intervent.*, **1**(4), pp. 395–402.
- [7] Suzuki, T., Mehta, R. H., Ince, H., Nagai, R., Sakomura, Y., Weber, F., Sumiyoshi, T., Bossone, E., Trimarchi, S., Cooper, J. V., Smith, D. E., Isselbacher, E. M., Eagle, K. A., and Nienaber, C. A., 2003, "Clinical Profiles and Outcomes of Acute Type B Aortic Dissection in the Current Era: Lessons From the International Registry of Aortic Dissection (IRAD)," *Circulation*, **108**(10, suppl. 1), pp. II–312.
- [8] Jonker, F. H., Patel, H. J., Upchurch, G. R., Williams, D. M., Montgomery, D. G., Gleason, T. G., Braverman, A. C., Sechtem, U., Fattori, R., Di Eusanio, M., Evangelista, A., Nienaber, C. A., Isselbacher, E. M., Eagle, K. A., and Trimarchi, S., 2015, "Acute Type B Aortic Dissection Complicated by Visceral Ischemia," *J. Thorac. Cardiovasc. Surg.*, **149**(4), pp. 1081–1086.
- [9] Fann, J. I., Sarris, G. E., Mitchell, R. S., Shumway, N. E., Stinson, E. B., Oyer, P. E., and Miller, D. C., 1990, "Treatment of Patients With Aortic Dissection Presenting With Peripheral Vascular Complications," *Ann. Surgery*, **212**(6), pp. 705–713.
- [10] Williams, D. M., Lee, D. Y., Hamilton, B. H., Marx, M. V., Narasimham, D. L., Kazanjian, S. N., Prince, M. R., Andrews, J. C., Cho, K. J., and Deeb, G. M., 1997, "The Dissected Aorta: Part III. Anatomy and Radiologic Diagnosis of Branch-Vessel Compromise," *Radiology*, **203**(1), pp. 37–44.
- [11] Chen, D., Müller-Eschner, M., Kotelis, D., Böckler, D., Ventikos, Y., and Tengg-Koblick, H. V., 2013, "A Longitudinal Study of Type-B Aortic Dissection and Endovascular Repair Scenarios: Computational Analyses," *Med. Eng. Phys.*, **35**(9), pp. 1321–1330.
- [12] Abazari, M. A., Rafieianzab, D., Soltani, M., and Alimohammadi, M., 2021, "The Effect of Beta-Blockers on Hemodynamic Parameters in Patient-Specific Blood Flow Simulations of Type-B Aortic Dissection: A Virtual Study," *Sci. Rep.*, **11**(1), pp. 1–14.
- [13] Menichini, C., Cheng, Z., Gibbs, R. G., and Xu, X. Y., 2016, "Predicting False Lumen Thrombosis in Patient-Specific Models of Aortic Dissection," *J. R. Soc. Interface*, **13**(124), p. 20160759.
- [14] Osswald, A., Karmonik, C., Anderson, J. R., Rengier, F., Karck, M., Engelke, K., Kallenbach, K., Kotelis, D., Partovi, S., Böckler, D., and Ruppert, A., 2017, "Elevated Wall Shear Stress in Aortic Type B Dissection May Relate to Retrograde Aortic Type A Dissection: A Computational Fluid Dynamics Pilot Study," *Eur. J. Vasc. Endovascular Surg.*, **54**(3), pp. 324–330.
- [15] Dillon-Murphy, D., Noorani, A., Nordsletten, D., and Figueroa, C. A., 2016, "Multi-Modality Image-Based Computational Analysis of Haemodynamics in Aortic Dissection," *Biomech. Model. Mechanobiol.*, **15**(4), pp. 857–876.
- [16] Cheng, Z., Riga, C., Chan, J., Hamady, M., Wood, N. B., Cheshire, N. J., Xu, Y., and Gibbs, R. G., 2013, "Initial Findings and Potential Applicability of Computational Simulation of the Aorta in Acute Type B Dissection," *J. Vasc. Surg.*, **57**(2), pp. 355–435.
- [17] Ahmed, S. B., Dillon-Murphy, D., and Figueroa, C. A., 2016, "Computational Study of Anatomical Risk Factors in Idealized Models of Type B Aortic Dissection," *Eur. J. Vasc. Endovascular Surg.*, **52**(6), pp. 736–745.
- [18] Cheng, Z., Wood, N. B., Gibbs, R. G., and Xu, X. Y., 2015, "Geometric and Flow Features of Type B Aortic Dissection: Initial Findings and Comparison of Medically Treated and Stented Cases," *Ann. Biomed. Eng.*, **43**(1), pp. 177–189.

- [19] Alimohammadi, M., Sherwood, J. M., Karimpour, M., Agu, O., Balabani, S., and Díaz-Zuccarini, V., 2015, "Aortic Dissection Simulation Models for Clinical Support: Fluid-Structure Interaction Vs. Rigid Wall Models," *Biomed. Eng. Online*, **14**(1), pp. 1–16.
- [20] Bonfanti, M., Balabani, S., Greenwood, J. P., Puppala, S., Homer-Vanniasinkam, S., and Díaz-Zuccarini, V., 2017, "Computational Tools for Clinical Support: A Multi-Scale Compliant Model for Haemodynamic Simulations in an Aortic Dissection Based on Multi-Modal Imaging Data," *J. R. Soc. Interface*, **14**(136), p. 20170632.
- [21] Qiao, Y., Zeng, Y., Ding, Y., Fan, J., Luo, K., and Zhu, T., 2019, "Numerical Simulation of Two-Phase Non-Newtonian Blood Flow With Fluid-Structure Interaction in Aortic Dissection," *Comput. Methods Biomech. Biomed. Eng.*, **22**(6), pp. 620–630.
- [22] Bonfanti, M., Balabani, S., Alimohammadi, M., Agu, O., Homer-Vanniasinkam, S., and Díaz-Zuccarini, V., 2018, "A Simplified Method to Account for Wall Motion in Patient-Specific Blood Flow Simulations of Aortic Dissection: Comparison With Fluid-Structure Interaction," *Med. Eng. Phys.*, **58**, pp. 72–79.
- [23] Qiao, A., Yin, W., and Chu, B., 2015, "Numerical Simulation of Fluid-Structure Interaction in Bypassed DeBakey III Aortic Dissection," *Comput. Methods Biomech. Biomed. Eng.*, **18**(11), pp. 1173–1180.
- [24] Bäuml, K., Vedula, V., Sailer, A. M., Seo, J., Chiu, P., Mistelbauer, G., Chan, F. P., Fischbein, M. P., Marsden, A. L., and Fleischmann, D., 2020, "Fluid-Structure Interaction Simulations of Patient-Specific Aortic Dissection," *Biomech. Model. Mechanobiol.*, **19**(5), pp. 1607–1628.
- [25] Roccabianca, S., Figueroa, C. A., Tellides, G., and Humphrey, J. D., 2014, "Quantification of Regional Differences in Aortic Stiffness in the Aging Human," *J. Mech. Behav. Biomed. Mater.*, **29**, pp. 618–634.
- [26] Vlachopoulos, C., O'Rourke, M., and Nichols, W. W., 2011, *McDonald's Blood Flow in Arteries: Theoretical, Experimental and Clinical Principles*, CRC Press, Boca Raton, FL.
- [27] Lantz, B. M., Foerster, J. M., Link, D. P., and Holcroft, J. W., 1981, "Regional Distribution of Cardiac Output: Normal Values in Man Determined by Video Dilution Technique," *Am. J. Roentgenol.*, **137**(5), pp. 903–907.
- [28] Hathcock, J. J., 2006, "Flow Effects on Coagulation and Thrombosis," *Arterioscler., Thrombosis, Vascular Biol.*, **26**(8), pp. 1729–1737.
- [29] Jouppila, P., and Kirkinen, P., 1984, "Increased Vascular Resistance in the Descending Aorta of the Human Fetus in Hypoxia," *BJOG Int. J. Obstetrics Gynaecol.*, **91**(9), pp. 853–856.
- [30] Gouloupoulou, S., and Webb, R. C., 2014, "Symphony of Vascular Contraction: How Smooth Muscle Cells Lose Harmony to Signal Increased Vascular Resistance in Hypertension," *Hypertension*, **63**(3), pp. e33–e39.
- [31] Humphrey, J. D., Harrison, D. G., Figueroa, C. A., Lacolley, P., and Laurent, S., 2016, "Central Artery Stiffness in Hypertension and Aging: A Problem With Cause and Consequence," *Circ. Res.*, **118**(3), pp. 379–381.
- [32] Ruland, S., and Aiyagari, V., 2007, "Cerebral Autoregulation and Blood Pressure Lowering," *Hypertension*, **49**(5), pp. 977–978.
- [33] Arthurs, C. J., Lau, K. D., Asress, K. N., Redwood, S. R., and Figueroa, C. A., 2016, "A Mathematical Model of Coronary Blood Flow Control: Simulation of Patient-Specific Three-Dimensional Hemodynamics During Exercise," *Am. J. Physiol. Heart Circ. Physiol.*, **310**(9), pp. H1242–H1258.
- [34] Lau, K. D., and Figueroa, C. A., 2015, "Simulation of Short-Term Pressure Regulation During the Tilt Test in a Coupled 3D–0D Closed-Loop Model of the Circulation," *Biomech. Model. Mechanobiol.*, **14**(4), pp. 915–929.
- [35] Figueroa, C. A., Taylor, C. A., and Marsden, A. L., 2017, "Blood Flow," *Encyclopedia of Computational Mechanics*, 2nd ed., American Cancer Society, Atlanta, GA, pp. 1–31.
- [36] Ravera, M., Re, M., Deferrari, L., Vettoretti, S., and Deferrari, G., 2006, "Importance of Blood Pressure Control in Chronic Kidney Disease," *J. Am. Soc. Nephrol.*, **17**(4 suppl 2), pp. S98–S103.
- [37] Peskin, C. S., 2002, "The Immersed Boundary Method," *Acta Numer.*, **11**, pp. 479–517.
- [38] Quint, L. E., Platt, J. F., Sonnad, S. S., Deeb, G. M., and Williams, D. M., 2003, "Aortic Intimal Tears: Detection With Spiral Computed Tomography," *J. Endovascular Ther.*, **10**(3), pp. 505–510.
- [39] Khojinezhad, A., Walot, I., Kruse, M. J., Rapae, T., Donayre, C. E., and White, R. A., 2010, "Distribution of Intimomedial Tears in Patients With Type B Aortic Dissection," *J. Vascular Surg.*, **52**(3), pp. 562–568.
- [40] Taylor, C. A., and Figueroa, C. A., 2009, "Patient-Specific Modeling of Cardiovascular Mechanics," *Annu. Rev. Biomed. Eng.*, **11**(1), pp. 109–134.
- [41] Cuomo, F., Roccabianca, S., Dillon-Murphy, D., Xiao, N., Humphrey, J. D., and Figueroa, C. A., 2017, "Effects of Age-Associated Regional Changes in Aortic Stiffness on Human Hemodynamics Revealed by Computational Modeling," *PLoS One*, **12**(3), p. e0173177.